Ecological Applications, 14(4) Supplement, 2004, pp. S22–S32

SEASONALITY OF WATER AND HEAT FLUXES OVER A TROPICAL FOREST IN EASTERN AMAZONIA

HUMBERTO R. DA ROCHA,[1,3] MICHAEL L. GOULDEN,[2] SCOTT D. MILLER,[2] MARY C. MENTON,[2] LEANDRO D. V. O. PINTO,[1] HELBER C. DE FREITAS,[1] AND ADELAINE M. E SILVA FIGUEIRA[1]

[1]*Department of Atmospheric Sciences, IAG/University of São Paulo, Rua do Matão, 1226, São Paulo, SP, Brazil, CEP 05508-900*

[2]*Department of Earth System Science, University of California, Irvine, California 92697-3100 USA*

Abstract. We used the eddy covariance technique from July 2000 to July 2001 to measure the fluxes of sensible heat, water vapor, and CO_2 between an old-growth tropical forest in eastern Amazonia and the atmosphere. Precipitation varied seasonally, with a wet season from mid-December 2000 to July 2001 characterized by successive rainy days, wet soil, and, relative to the dry season, cooler temperatures, greater cloudiness, and reduced incoming solar and net radiation. Average evapotranspiration decreased from 3.96 ± 0.65 mm/d during the dry season to 3.18 ± 0.76 mm/d during the wet season, in parallel with decreasing radiation and decreasing water vapor deficit. The average Bowen ratio was 0.17 ± 0.10, indicating that most of the incoming radiation was used for evaporation. The Bowen ratio was relatively low during the early wet season (December–March), as a result of increased evaporative fraction and reduced sensible heat flux. The seasonal decline in Bowen ratio and increase in evaporative fraction coincided with an increase in ecosystem CO_2 assimilation capacity, which we attribute to the growth of new leaves. The evaporative fraction did not decline as the dry season progressed, implying that the forest did not become drought stressed. The roots extracted water throughout the top 250 cm of soil, and water redistribution, possibly by hydraulic lift, partially recharged the shallow soil during dry season nights. The lack of drought stress during the dry season was likely a consequence of deep rooting, and possibly vertical water movement, which allowed the trees to maintain access to soil water year round.

Key words: *Amazonia; eddy covariance; energy balance; evapotranspiration; hydraulic lift; LBA; soil moisture; tropical forest.*

INTRODUCTION

Tropical forests play a key role in the hydrology of Amazonia. About half of the moisture that falls in the Amazon basin originates from evapotranspiration off upwind forest, and the other half originates from evaporation off the tropical Atlantic Ocean (Nobre et al. 1991). The regional pattern of precipitation within Amazonia is linked to the large-scale pattern of land-surface evaporation. At the same time, the distribution of forest in the tropics is linked to rainfall, with closed-canopy evergreen forest occurring in areas with at least 2 m annual rainfall (Walter 1984). Amazonia is therefore best understood as a coupled system, where vegetation affects the patterns of precipitation (da Rocha et al. 1996*a*) and precipitation affects the distribution and activity of vegetation. One of the goals of the Large-scale Biosphere–Atmosphere Experiment in Amazonia (LBA) is an improved understanding of the components that determine this coupling, including the seasonal patterns of, and biological and physical controls on, forest evapotranspiration.

Early observations of forest evapotranspiration in Amazonia focused on the Manaus area, where Shuttleworth et al. (1984) and Fitzjarrald et al. (1988) used micrometeorological techniques during pioneering studies. Shuttleworth (1988) subsequently combined field measurements and model-based extrapolation to calculate the monthly variation of evaporation. Roberts et al. (1990) relied on methods from plant physiology to infer that primary forest is not very sensitive to seasonal soil moisture deficit. Nepstad et al. (1994) emphasized the role of deep roots in allowing evapotranspiration to continue during the dry season in large regions of Amazonia. Much of the early work on forest evaporation in Amazonia was done before year-round flux observation became feasible, and, consequently, was confined to relatively short intensive field campaigns. While the technical hurdles preventing year-round micrometeorological observation were largely resolved in the 1990s (Wofsy et al. 1993), recent work on forest–atmosphere exchange in the Amazon has focused on CO_2 exchange, rather than energy exchange (Fan et al. 1990, Grace et al. 1995, Malhi et al. 1998).

We established a micrometeorological field station in June 2000 to make continuous observations of the

Manuscript received 8 January 2002; accepted 10 June 2002; final version received 28 February 2003. Corresponding Editor: D. S. Schimel. For reprints of this Special Issue, see footnote 1, p. S1.

[3] E-mail: humberto@model.iag.usp.br

local climate and the fluxes of heat, water, and CO_2 between the atmosphere and a primary tropical forest in eastern Amazonia (Santarém, state of Pará, Brazil). In this paper, we focus on the diel and seasonal patterns of evapotranspiration, sensible heat flux, microclimate, and soil moisture observed from July 2000 to July 2001. Two companion papers (Goulden et al. 2004 and Miller et al. 2004) describe the experimental design in more detail and discuss the diel, seasonal, and annual patterns of CO_2 exchange.

Methods

Site

The measurements were made in the Floresta Nacional do Tapajós, near the km 83 marker on the Santarém-Cuiabá highway (BR 163), ~70 km south of Santarém, state of Pará, Brazil (3.01030° S, 54.58150° W). The vegetation was a tropical humid forest on a broad, flat plateau. The site was selectively logged in September 2001, but all of the observations reported here were made prior to the logging, while the vegetation was still old growth. The soil was a yellow latosol clay (Haplic acrorthox). Additional details of the landscape are reported by Hernandez Filho et al. (1993). Full descriptions of the experimental design and instrumentation are given by Goulden et al. (2004) and Miller et al. (2004).

Measurements

The flux measurements were made from a 67 m tall tower (Rohn 55G, Rohn, Peoria, Illinois, USA). The data acquisition computer and some of the instruments were operated in an air-conditioned hut 8 m south of the tower base. Power was provided by a diesel generator located 800 m south of the tower. The measurements discussed here were made from 1 July 2000 to 5 July 2001. Valid meteorological data were obtained during 91% of this period and valid surface fluxes were obtained during 85% of this period. One large data gap occurred in April 2001 when the sonic anemometer failed.

The data acquisition system used five networked data loggers (CR10x or CR23x; Campbell Scientific, Logan, Utah, USA), which delivered raw 4- or 0.5-Hz data to a computer on site. The wind and temperature at 64 m altitude were measured at 4 Hz with a three-axis sonic anemometer (Campbell Scientific). The CO_2 and H_2O densities at 64 m were measured with two independent infrared gas analyzers (an open-path Li-Cor 7500 and a closed-path Li-Cor 6262 or 7000; Li-Cor, Lincoln, Nebraska, USA). The current analysis relied most heavily on the fluxes calculated with the open path gas analyzer, which were judged more reliable for the humidity flux based on spectral analyses. The turbulent fluxes were calculated as the 30-min covariances of vertical wind velocity and either temperature or H_2O. The fluxes were rotated to the plane with no mean vertical wind (McMillen 1988).

Observations of the physical environment were recorded at 0.5 Hz, including precipitation at 64 m (TE525 rain gauge; Texas Electronics, Dallas, Texas, USA), incoming short-wave radiation at 64 m (CM6B pyranometer; Kipp & Zonen, Delft, The Netherlands), net radiation at 64 m (Q*7.1 ventilated net radiometer; REBS, Seattle, Washington, USA), soil moisture at 20 locations from 5- to 250-cm depth (Campbell Scientific CS615 water content reflectometers), and soil heat flux at 2 cm depth in five locations (REBS HFT3.1 heat flux plates).

Calibration curves for the soil moisture probes were developed using large blocks of soil collected at 5 cm and 25 cm depth. The calibrations were carried out by automated gravimetry in our laboratory at the University of São Paulo. Probes were inserted into intact blocks of soil that were shipped from the site. The soil was initially saturated and then allowed to dry gradually for several days with gentle indoor ventilation. The wave-guide transit time (sensor output) and the mass of the soil block were recorded every 20 min until no significant variations were observed. The sample was then dried in an oven at 108°C to correct for the remaining water content. The calibration curve was θ (m^3/m^3) = $2.745 - 9.429t + 10.212t^2 - 3.297t^3$ (R^2 = 0.97) for soil collected at 5 cm, and θ (m^3/m^3) = $1.759 - 6.830t + 8.114t^2 - 2.790t^3$ (R^2 = 0.98) for soil collected at 25 cm, where t is the transit time in ms.

Data analysis

Energy budget closure provides a measure of the absolute accuracy of the measured fluxes of sensible heat flux (H) and latent energy (LE). If all measurements are accurate, the energy budget should close such that

$$(R_n - G - S_{bc} - C - A) \approx (H + \mathrm{LE}) \quad (1)$$

where R_n is the measured net radiation, G is the measured soil heat flux, S_{bc} is the energy stored in biomass and canopy air beneath 64 m, C is the chemical energy for net CO_2 exchange, and A is the energy advected by horizontal wind. R_n, G, H, and LE were measured directly. S_{bc} was calculated using the empirical relationships reported by Moore and Fisch (1986) for tropical forest in Manaus:

$$S_c = S_T + S_q = 16.7\Delta T_r + 28.0\Delta q_r \quad (2)$$

$$S_b = 12.6\Delta T_{r*} \quad (3)$$

where S_T and S_q are the sensible heat and latent heat storage in the canopy air column (W/m^2), S_b is the energy stored in the biomass (W/m^2), ΔT_r is the hourly change in air temperature (K), Δq_r is the hourly change in specific humidity (g water/kg air), and ΔT_{r*} is the hourly change lagged one hour. Advection (A) is very

difficult to measure, and is hypothesized to be insignificant over homogeneous, flat terrain. Chemical storage (C) is generally small, and was not considered.

The Penman-Monteith equation describes the dependence of evaporation on the meteorological (air temperature and humidity, available energy, and wind speed) and biological (canopy stomatal conductance) conditions. In studies where the evaporation and meteorological conditions are independently measured, the Penman-Monteith equation can be inverted to calculate the canopy conductance to water vapor (g_c), which is analogous to stomatal conductance on a ground-area basis. The canopy conductance, and the aerodynamic conductance to water vapor (g_{av}), which describes the turbulent transport from 64 m to the outside of the leaf boundary layers, were calculated as

$$\frac{1}{g_c} = r_c = \frac{r_{av}}{\gamma}\left[\frac{\Delta(R_n - G) + \rho c_p \delta e g_{av}}{LE} - (\Delta + \gamma)\right] \quad (4)$$

$$\frac{1}{g_{av}} = r_{av} = \frac{u}{u^{*2}} + \frac{1}{ku^*}\left[\ln\left(\frac{z_0}{z_v}\right) + \Psi_m - \Psi_v\right] \quad (5)$$

where R_n is the net radiation, G is the soil heat flux, LE is the flux of latent energy, ρ is the air density, c_p is specific heat at constant pressure, δe is the water vapor pressure deficit, Δ is the rate of change of saturated water vapor pressure with temperature, $\gamma = (pc_p/\varepsilon L)$, L is the latent heat of vaporization, p is the atmospheric pressure, and $\varepsilon = 0.622$. The variables Ψ_v and Ψ_m in the right-hand side of Eq. 5 account for the effects of atmospheric stability and were calculated following Verma (1989). The ratio $\ln(z_0/z_v)$ was set to 2 following Garratt (1992) and Grace et al. (1995); z_0 is the aerodynamic roughness length (a measure of how rough the top of the canopy is and its effectiveness in retarding the flow of the overlying air) and z_v is the roughness length for water vapor.

Results and Discussion

Climate and radiation

The local climate was hot and humid, with reduced rainfall from August to December (Fig. 1a). The total precipitation from 1 July 2000 to 1 July 2001 was 2200 mm, though this sum may underestimate the true precipitation as a result of observational gaps. About one-third of the annual precipitation fell from 15 July to 14 December, with the remainder falling from late December to July. In subsequent analyses we refer to the period 15 July to 14 December as the dry season and to the remaining period as the wet season. There was a tendency for increased precipitation from 1300 and 1600 hours local time, presumably as a result of increased convection (Fig. 2b). Intense rainfall occurred occasionally during the dry season. The wet season was marked by many consecutive days with moderate rainfall (Figs. 1a and 2c).

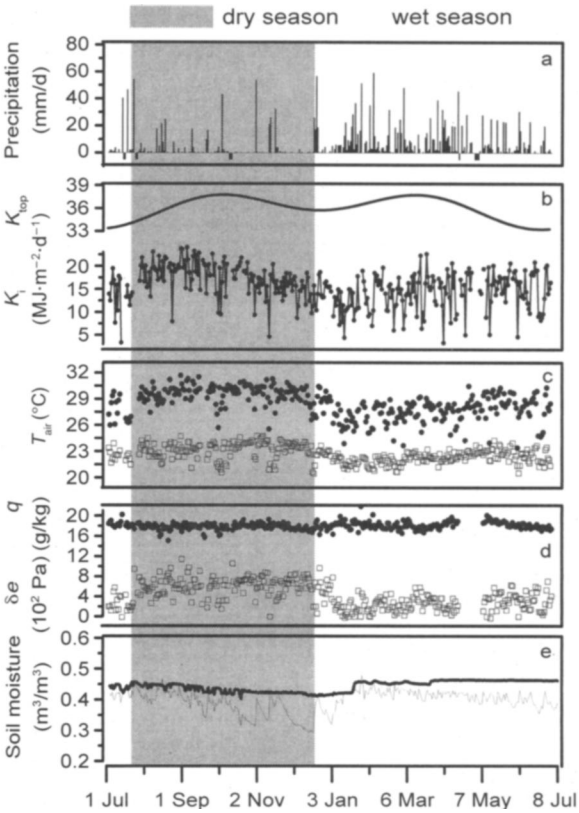

FIG. 1. (a) Daily precipitation at 64 m (negative bars are missing values). (b) Daily mean solar radiation at 64 m (K_i; lines connecting filled cirlces) and calculated daily mean solar radiation at the top of the atmosphere (K_{top}; solid line). (c) Maximum (filled circles) and minimum (open squares) air temperature at 64 m. (d) Daily mean specific humidity (q; lines connecting filled circles), and daily mean water vapor pressure deficit (δe; open squares). (Note that the scale for δe is in hundreds of pascals.) (e) Daily mean volumetric soil moisture at 5 cm depth (thin solid line) and at 250 cm depth (thick solid line). All data are calculated for 24-h periods from 1 July 2000 to 5 July 2001. The dry season is shaded.

The horizontal wind at 64 m was generally from the east at 1–3 m/s (Miller et al. 2004). The local winds are a consequence of larger atmospheric circulations, including the Intertropical Convergence Zone and the South Atlantic Convergence Zone (Peixoto and Oort 1994). The prevailing surface winds result from the trade winds and the northern branch of the semipermanent high pressure in the South Atlantic Ocean. The site is 14 km east of the Tapajós River, which creates a river circulation that shifts the wind to a westerly flow on some afternoons in the dry season. Cold fronts from the south reach the region several times a year, resulting in slightly cooler temperatures and a shift to westerly winds.

Calculated solar radiation at the top of atmosphere (Stull 1994) (K_{top} in Fig. 1b) had two maxima (22 September and 22 March) and two minima (22 June and

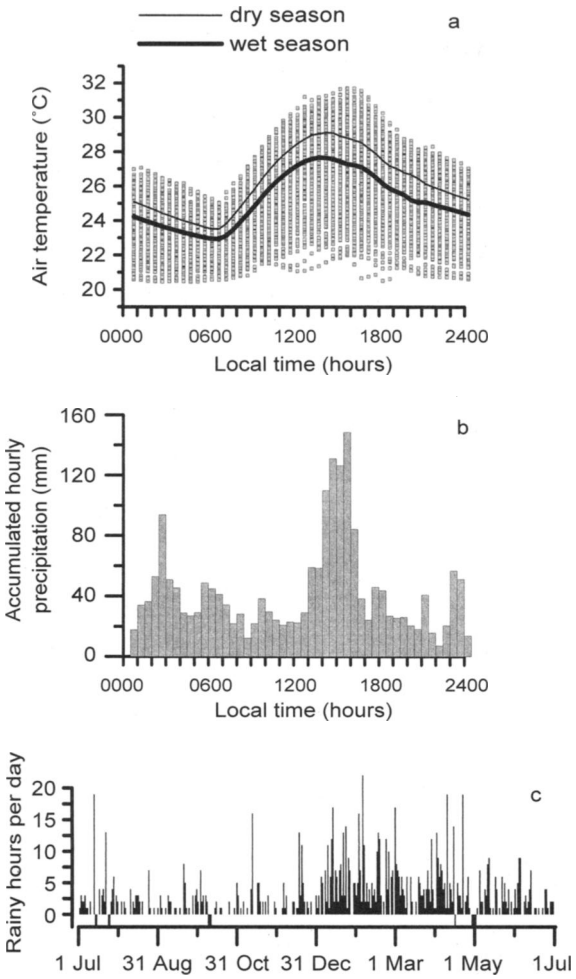

FIG. 2. (a) Diel pattern of air temperature at 64 m (30-min average). The thin solid line shows the dry season average (20 July–14 December 2000); the thick solid line shows the wet season average (1–13 July 2000 and 15 December 2000–30 June 2001). (b) Diel pattern of accumulated hourly precipitation. (c) Number of rainy hours per day (negative bars are missing values).

a secondary minimum on 22 December). Incoming solar radiation varied seasonally, reaching a maximum of ~24 MJ·m^{-2}·d^{-1} in September and a minimum of 8–12 MJ·m^{-2}·d^{-1} at the beginning of the wet season (Fig. 1b). Seasonal change in cloud cover was the main controller of incident radiation, with solar angle playing a secondary role. The transition from dry to wet season coincided with a marked reduction in incoming radiation.

The surface air temperature varied little over the year (Fig. 1c), a pattern that is typical for the region (Culf et al. 1996). The maximum daily temperature was 24–32°C and the minimum was 20–25°C (Figs. 1c and 2a). The dry season was 1–3°C warmer on average than the wet season. A few periods with cooler than average temperatures were observed during the dry season, reflecting the incursion of cold fronts from the south. The daily maximum and minimum temperatures and the daily temperature range were reduced during the three months centered on January (Fig. 1c), coincident with increased cloudiness. The water vapor content in the air was consistently 17–19 g water/kg air (Fig. 1d). The daily average water vapor deficit decreased from 700 Pa in the dry season to 200 Pa in the wet season (Fig. 1d), coincident with the decline in daytime air temperature.

Soil moisture

Shallow (5 cm beneath the surface) soil moisture ranged from 0.47 m^3 water/m^3 soil in the wet season to 0.3 m^3 water/m^3 soil in the dry season (Fig. 1e). Deep (250 cm beneath the surface) soil moisture was comparatively constant year round, ranging from 0.46 m^3 water/m^3 soil in the wet season to 0.42 m^3 water/m^3 soil late in the dry season. The shallow soil moisture varied markedly during the dry season in response to storms, while the deep soil moisture declined gradually during the dry season.

The soil moisture content late in the dry season increased with depth from 0.356 m^3 water/m^3 soil at 5 cm to 0.414 m^3 water/m^3 soil at 200 cm (Fig. 3). Both the shallow and deep soil moisture showed regular diel

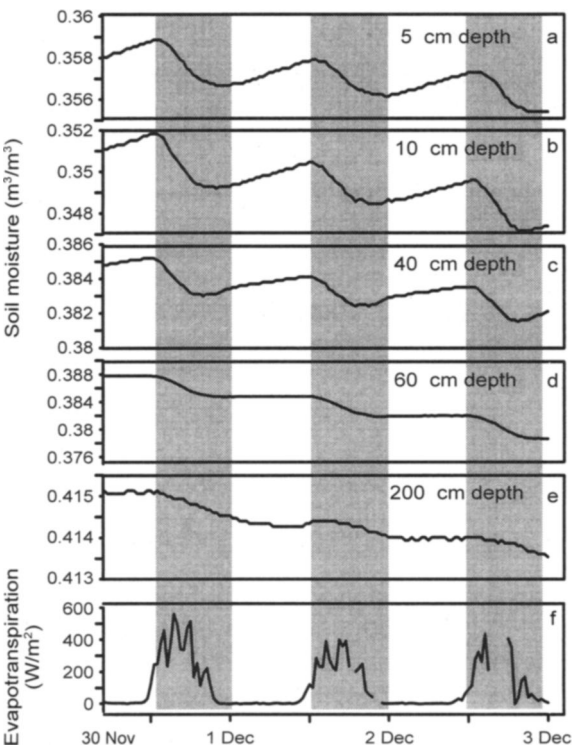

FIG. 3. Soil moisture (30-min means) at (a) 5, (b) 10, (c) 40, (d) 60, and (e) 200 cm beneath the soil surface. (f) Evaporation, measured by eddy covariance. The observations were made during a rain-free period late in the 2000 dry season (30 November–2 December).

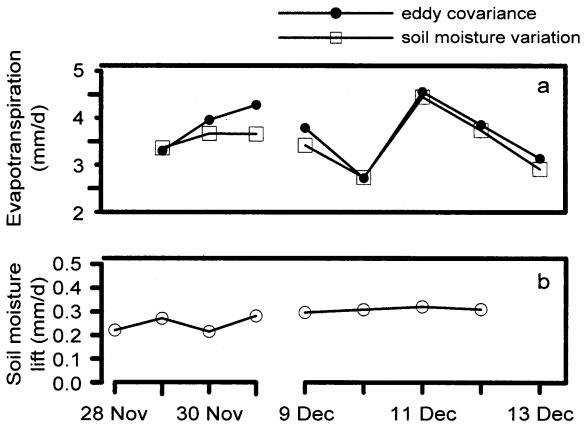

FIG. 4. (a) Daily evaporation, calculated from soil moisture withdrawal in the upper 250 cm of soil (solid line connecting open squares) and from the eddy covariance measurements (solid line connecting filled circles). (b) Nocturnal soil moisture lift in the upper 60 cm of soil (solid line connecting open circles). Measurements were made during rain-free periods late in the 2000 dry season (28–30 November, 1 December, and 9–12 December 2000).

patterns of moisture withdrawal during extended periods without rain (Fig. 3). The daily withdrawal of water in early December declined with depth from 0.001 to 0.002 m^3 water·m^{-3} soil·d^{-1} in the upper 160 cm of soil to 0.0005 m^3 water·m^{-3} soil·d^{-1} at 200 cm depth (Fig. 3). The pattern of water withdrawal with depth presumably reflects the distribution of root activity, with fewer active roots beneath 1.6 m depth. The daily total withdrawal of water in the upper 2 m of soil was 2.5 to 4.5 mm/d, which is in excellent agreement with the daily evaporation measured simultaneously by eddy covariance (Fig. 4a). The soil moisture content at 2 m decreased moderately during daytime and remained relatively constant at night. This diel pattern implies significant extraction of water by roots at 2 m depth (Fig. 3). The day-to-day extraction of deep water remained constant as the dry season progressed, and the soil at 2 m remained moist year round, implying that the trees maintained access to soil water throughout the dry season (Figs. 1e, 3, 4a).

The shallow soil water content during rain-free periods decreased during daytime and recovered partially during nighttime (Fig. 3), a pattern that we attribute to the nocturnal redistribution of water. Lopes (2001) reported a similar nocturnal recovery for both tropical forest and grassland growing on silt–clay podzols in southern Amazonia. The nocturnal redistribution of soil water can occur either by flow through plant roots, a process referred to as hydraulic lift (Caldwell et al. 1998), or flow through the bulk soil. Hydraulic lift occurs when root systems provide a low-resistance bridge between shallow dry soil and deep moist soil. Water flows through roots from moist, deep soil to shallow dry soil at night, resulting in an increase in shallow-soil water content. Hydraulic lift has been reported in semiarid shrublands, conifer and temperate forests, and several types of cropland. Nocturnal soil moisture redistribution can also occur by capillary flow through the bulk soil in response to strong vertical gradients in matric potential.

The nocturnal recharge integrated throughout the top 60 cm of soil was 0.3 mm/d (Fig. 4b). This rate of recharge is equivalent to 10% of the daily evapotranspiration (Fig. 4a). The nocturnal recharge may be important for forest function. The redistribution of water may help the trees avoid drought stress by increasing the efficiency with which deep roots extract water. Likewise, redistribution may increase microbial activity in the shallow soil by improving the local moisture status.

Energy balance

Energy budget closure provides a measure of the absolute accuracy of the measured fluxes of sensible heat flux (H) and latent energy (LE) (Fig. 5). Energy storage associated with changes in the temperatures of trunks and stems and in the temperature and humidity of air within the canopy can be substantial in tall forest. While this storage approaches zero when integrated over 24 h, the daytime magnitude can significantly affect the amount of available energy (the net radiation after subtracting the energy stored). From 2 to 6 W/m^2 of energy was stored in the biomass during daytime, and a comparable amount of energy was released from the biomass at night (Fig. 6). Similarly, 0–3 W/m^2 was stored in the air column during daytime and lost at night. The seasonality of the canopy energy storage followed the variation of the daily air temperature

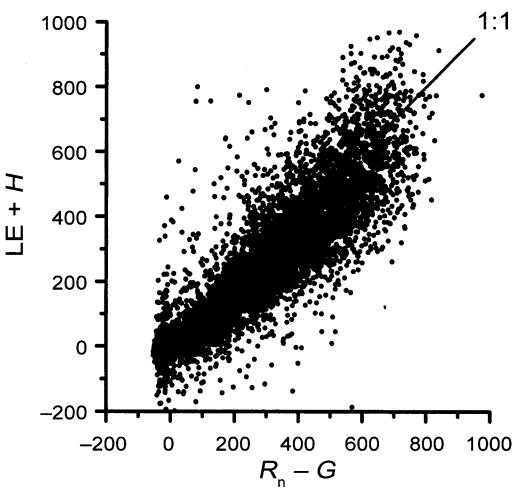

FIG. 5. Available energy (net radiation [R_n] minus the sum [G] of soil heat flux, biomass heat storage, and canopy heat storage) plotted against the sum of latent (LE) and sensible heat (H) flux ($Y = 0.864\ X + 10.3$, $R^2 = 0.86$, $n = 14\,064$ points).

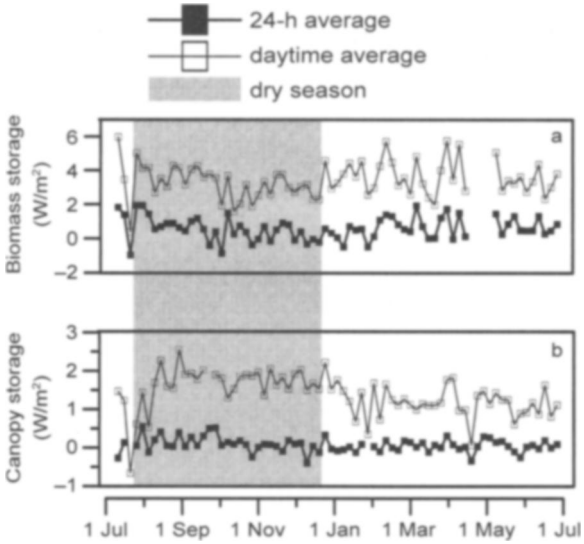

FIG. 6. (a) Biomass energy storage averaged over 24 h (line connecting filled squares for 5-d means) and averaged over the 12 daytime hours (line connecting open squares). (b) Canopy energy storage averaged over 24 h (line connecting filled squares) and averaged over the 12 daytime hours (line connecting open squares). The dry season is shaded.

range, with a decrease in the wet season and an increase in the dry season (Figs. 1c, 6b).

The energy budget indicated that turbulent exchange underestimated available energy by 13% (Fig. 5). Our failure to completely close the energy budget is consistent with observations from many other sites. The discrepancy is unlikely to result from uncertainty in the soil heat flux, since the soil heat flux was only 2% of the daytime net radiation. Moreover, the fraction G/R_n observed is typical for closed-canopy forests (Alvala et al. 1996). The analysis of the energy budget suggests that the turbulent fluxes reported here may underestimate the true fluxes by about 13%, or possibly more depending on the accuracy of the net radiation measurement. This possibility should be kept in mind when interpreting the results, including the annual integrated evaporation.

Seasonal patterns of water and heat fluxes

Ecosystem evaporation represents the sum of evaporation from soil surfaces, leaves during gas exchange, and plant surfaces following precipitation. The evaporation ranged from 1.5 to 6 mm/d, with an annual average of 3.45 ± 0.81 mm/d. The annually integrated evaporation was ~1300 mm, or 60% of the observed precipitation. Evaporation and sensible heat flux increased in the dry season and decreased in the wet season, coincident with changes in cloudiness and net radiation (Fig. 7). The observed evaporation is comparable to the rate of 3.5 mm/d reported by Shuttleworth (1988), which was based on a combination of observations and model runs for a forest near Manaus. The observed evaporation is also comparable to the annual rate of 3.7–4.0 mm/d reported by da Rocha et al. (1996*b*), which was based on model runs for three forest sites in Amazonia (Grace et al. 1995, Gash et al. 1996, Sellers et al. 1996). The observed increase in evaporation in the dry season is similar to that predicted by Shuttleworth (1988) and da Rocha et al. (1996*b*).

Daily integrated net radiation was the main controller of day-to-day variation in latent and sensible heat flux, with high turbulent fluxes occurring on sunny days. The 24-h average net radiation was 70–180 W/m², with an average of 140 W/m² in the dry season and 113 W/m² in the wet season (Fig. 7a and Table 1). The inter- and intraseasonal patterns of latent and sensible heat flux were similar to the trends in radiation (Fig. 7a–c). Evaporation was relatively high (~4 mm/d; Table 1) and constant from day to day in the dry season (CV = 16%), and low (~3.2 mm/d) and variable in the wet season (CV = 25%). Likewise, net radiation was relatively constant from day to day in the dry season and variable in the wet season. The seasonal pattern of sensible heat flux was broadly similar to the seasonal pattern of radiation, with a minimum centered in January. The 24-h average heat flux was 21 W/m² in the dry season and 16 W/m² in the wet season. The variance in H was slightly larger in the wet season than the dry season, a pattern that we attribute to the variance in radiation (Table 1).

While daily integrated radiation was the main controller of daily evaporation, it did not explain all of the day-to-day variance. The evaporative fraction, calcu-

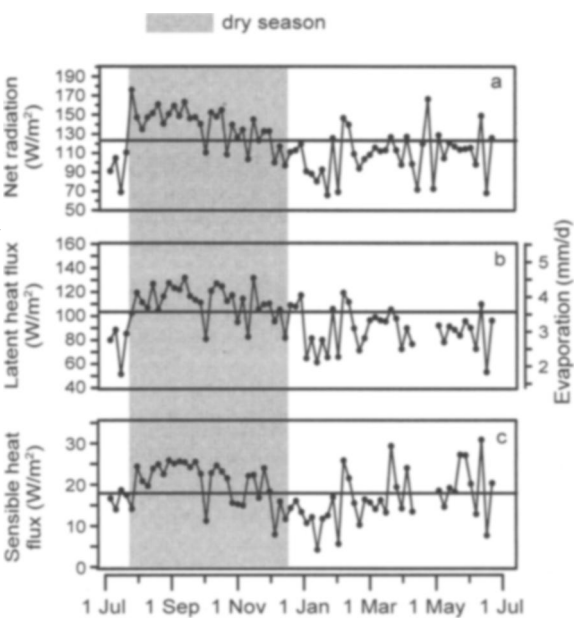

FIG. 7. (a) Net radiation (lines connecting 5-d means), (b) latent heat flux (on the left axis) and evaporation (on the right axis), and (c) sensible heat flux. The horizontal lines represent the annual means. The dry season is shaded.

TABLE 1. Averages (over 24 h) ± 1 SD of evapotranspiration (E), net radiation (R_n), sensible heat flux (H), global solar radiation (K_i), Bowen ratio (H/LE), evaporative fraction (LE/R_n), surface conductance (g_c), aerodynamic conductance to water vapor (g_{av}), soil heat flux (G), friction velocity (u^*), and 64-m wind speed.

Season	E (mm/d)	R_n (W/m^2)	H (W/m^2)	K_i (W/m^2)	Bowen ratio (H/LE)
Dry season	3.96 ± 0.65	140.3 ± 26.4	20.7 ± 9.3	203.5 ± 39.9	0.17 ± 0.08
Wet season	3.18 ± 0.67	112.6 ± 32.0	16.4 ± 10.4	165.2 ± 45.7	0.17 ± 0.11
All year	3.51 ± 0.75	123.5 ± 32.5	18.1 ± 10.1	180.0 ± 46.8	0.17 ± 0.10
Transition, dry-to-wet season	...	...	13.3 ± 9.8	...	0.14 ± 0.09

Note: The dry-season averages were calculated from 20 July to 14 December 2000; the wet-season averages were calculated from 1–13 July 2000 and 15 December 2000 to 30 June 2001; the transition dry-to-wet season averages were calculated from 15 December 2000 to 15 February 2001.

lated as the percentage ratio of latent heat flux to net radiation, varied seasonally, reaching a minimum of 65–75% from May to October and a maximum of 75–100% from December to March (Fig. 8a). Likewise, the Bowen ratio (sensible heat flux divided by latent heat flux, a measure of energy partitioning) varied seasonally, with a minimum coinciding with the maximum evaporative fraction (Fig. 8b). The increase in evaporative fraction from December to March cannot be explained based on a seasonal change in potential evaporation. The water vapor pressure deficit was relatively low during much of this period (Fig. 8c), as a result of cooler air temperatures (Fig. 1c). The direct effect of a decrease in water vapor pressure deficit is a decrease in evaporative fraction and an increase in Bowen ratio, which are opposite the trends observed.

The seasonal shift in energy partitioning may be partially related to the frequency of precipitation (see Fig. 2c). Frequent, moderate- to light-intensity storms increase the overall fraction of precipitation retained on plant surfaces. This intercepted precipitation subsequently evaporates rapidly, since there is no stomatal limitation, resulting in higher overall rates of evaporation. In contrast, heavy, infrequent storms increase the fraction of precipitation that infiltrates into soil. The seasonal shift in rainfall frequency (Figs. 1a, 2c) may partially explain the decrease in Bowen ratio and increase in evaporative fraction observed early in the rainy season (Fig. 8a, b). Rain fell very frequently during this period (Figs. 1a, 2c), a pattern that should result in higher rates of evaporation by increasing the fraction of interception loss.

The seasonal pattern of energy exchange was probably also controlled in part by changes in tree physiology. The decline in evaporative fraction in May preceded the onset of the dry season, and the increase in evaporative fraction in November preceded the end of the dry season (Figs. 1e, 8a), indicating that the seasonal pattern of evaporative fraction cannot be explained entirely by changes in meteorology. The canopy surface conductance (g_c), which is analogous to stomatal conductance on a ground-area basis, provides a useful measure of the effect of physiology on energy exchange. The canopy surface conductance was comparatively large from December until early April (Fig. 9), suggesting that the seasonal changes in evaporative fraction and Bowen ratio were caused in part by changes in leaf area index (LAI) or leaf physiology. The seasonal patterns of evaporative fraction, Bowen ratio, and canopy conductance are broadly similar to the seasonal pattern of daytime CO_2 uptake described for the site by Goulden et al. (2004). Goulden et al. found that CO_2 uptake at a given light intensity was greater from October to April than from May to September, a pattern they attributed to a seasonal increase in LAI. It is likely that these observations are related, and that the October-to-April increases in canopy photosynthesis, canopy conductance, and evaporative fraction, and decrease in Bowen ratio, are mechanistically linked through seasonal changes in LAI.

Diel patterns of water and heat fluxes

The diel patterns of latent and sensible heat flux (Fig. 10a, b) were closely tied to the intensity of sunlight. The sensible heat flux reached a maximum before noon local time, and was typically negative at night. The latent heat flux reached a maximum shortly after noon local time, and approached zero at night. The sensible heat flux peaked at <300 W/m^2, with a dry season 24-h average of 21 W/m^2 and a wet season 24-h average of 18 W/m^2 (Fig. 10b, Table 1). Latent heat flux peaked at 800 W/m^2, with a wet season 24-h average of 92 W/m^2 and a dry season 24-h average of 115 W/m^2 (Fig. 10a, Table 1). The integrated daily Bowen ratio was 0.17 over the year, indicating that most of the incoming solar energy was used to evaporate water (Fig. 10c, Table 1).

The aerodynamic conductance (g_{av}) varied diurnally, reaching a minimum at night and a maximum shortly before noon (Fig. 11b). The peak is strongly correlated with a similar peak in the horizontal wind speed at 64 m at the same hour (not shown). The aerodynamic conductance increased rapidly in the morning, when thermal instability caused by increasing solar energy eroded the previous night's stable boundary layer and caused rapid mixing above the forest. The diel pattern of g_{av} varied seasonally, with a faster increase in the first hours of daytime in the dry season than the wet

TABLE 1. Extended.

Evaporative fraction (LE/R_n)	g_c (mm/s)	g_{av} (mm/s)	G (W/m^2)	u^* (m/s)	64-m wind speed (m/s)
0.83 ± 0.1	12.2 ± 3.5	28.9 ± 6.9	0.1 ± 2.8	0.29 ± 0.05	2.9 ± 0.4
0.87 ± 0.31	13.0 ± 4.9	28.5 ± 7.6	1.2 ± 2.4	0.28 ± 0.06	2.5 ± 0.5
0.86 ± 0.28	12.7 ± 4.4	28.7 ± 7.3	0.8 ± 2.6	0.29 ± 0.06	2.6 ± 0.5
0.91 ± 0.23	14.9 ± 5.1	...	...	...	...

season. The increased morning g_{av} during the dry season may result from an increase in daytime radiation, which should generate greater kinetic energy in the boundary layer. Alternatively, the seasonal trend in g_{av} may be a result of a regional trend toward increased kinetic energy during the austral winter and spring (Peixoto and Oort 1994).

The canopy conductance g_c generally peaked before noon and declined in the afternoon (Fig. 11a), a pattern similar to that observed at other Amazonian sites (Shuttleworth 1988, Grace et al. 1995). This diel pattern was broadly similar to that of g_{av}, reaching a minimum at night and a maximum shortly before noon. The peak g_c was ~24 mm/s on average, which is a factor of ~2.5 less than the peak g_{av}, indicating substantial stomatal limitation to evaporation. The surface conductance declined in the afternoon, presumably as a result of stomatal closure (Fig. 11c). Goulden et al. (2004) analyzed data from the same site and found that canopy CO_2 uptake reached a maximum at around 1000 local time, and declined steadily in the afternoon. Goulden et al. attributed the afternoon decline to either stomatal closure caused by high evaporative demand, or an effect of high temperature on photosynthetic biochemistry, or an intrinsic circadian rhythm, or a combination of the three. The afternoon decline in g_c in Fig. 11 corresponds well with the decline in CO_2 uptake reported by Goulden et al. (2004). These two phenomenon are likely related, though we are unable to identify the specific causal mechanism.

The Bowen ratio increased shortly after sunrise and reached a maximum in the morning, before declining in the afternoon (Fig. 10c). The diurnal change in Bowen ratio resulted from a slight asynchrony between the energy fluxes, with the sensible heat flux peaking earlier in the day than the latent heat flux (Fig. 10a, b). The diel trend in Bowen ratio resulted from the diel patterns of air temperature (Fig. 2a) and vapor pressure deficit (Fig. 11c). The observed afternoon decline of g_c (Fig. 11a) would be expected to increase the Bowen

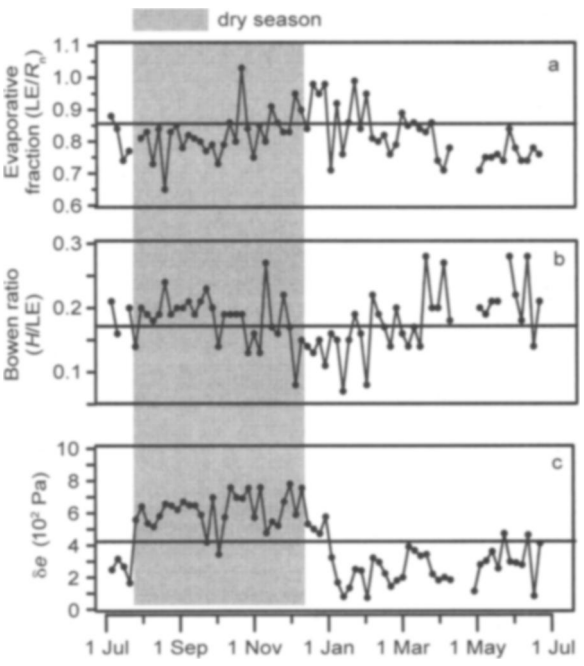

FIG. 8. (a) Evaporative fraction (daytime latent heat flux divided by net radiation; lines connecting 5-d means), (b) Bowen ratio (ratio of daytime sensible heat flux to latent heat flux), and (c) water vapor pressure deficit (note that the scale is in hundreds of pascals). The horizontal lines represent the annual means. The dry season is shaded.

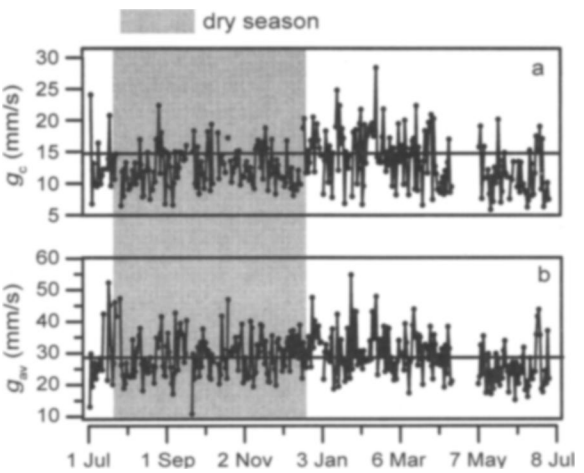

FIG. 9. (a) Surface conductance (g_c; 24-h averages connected by lines) and (b) aerodynamic conductance of water vapor (g_{av}) from 1 July 2000 to 30 June 2001. The horizontal lines represent the annual means. The dry season is shaded.

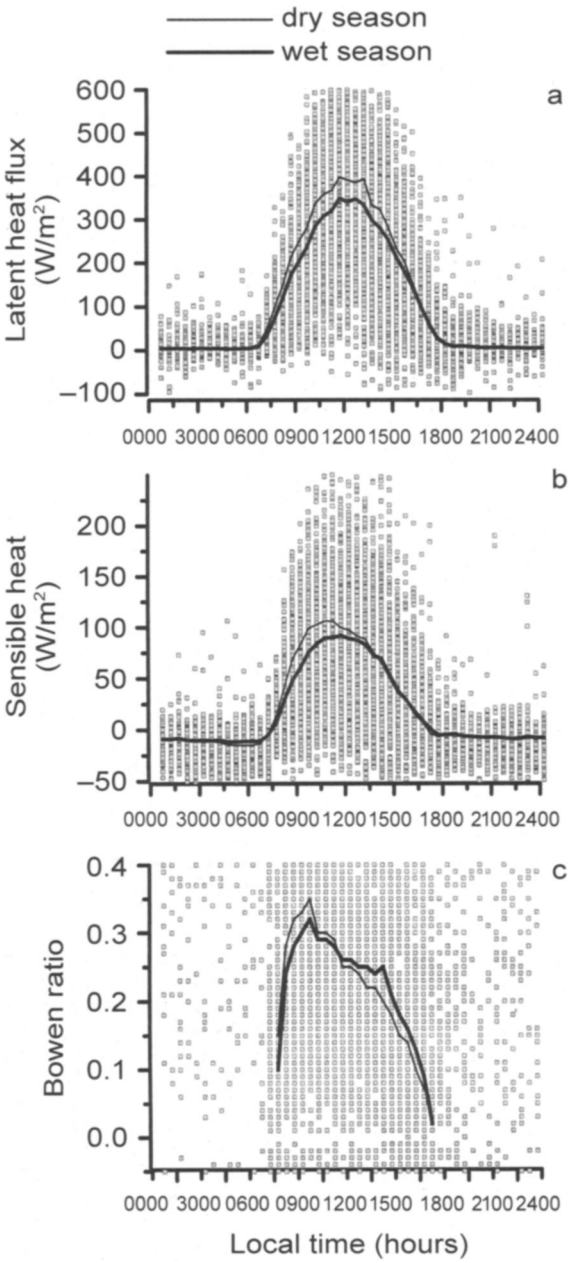

FIG. 10. Diel patterns of (a) latent heat flux (LE), (b) sensible heat flux (H), and (c) Bowen ratio (the ratio of H to LE). Curves are 30-min means calculated separately for the dry season (thin solid line; 20 July–14 December 2000) and the wet season (thick solid line; 1–13 July 2000 and 15 December 2000–30 June 2001).

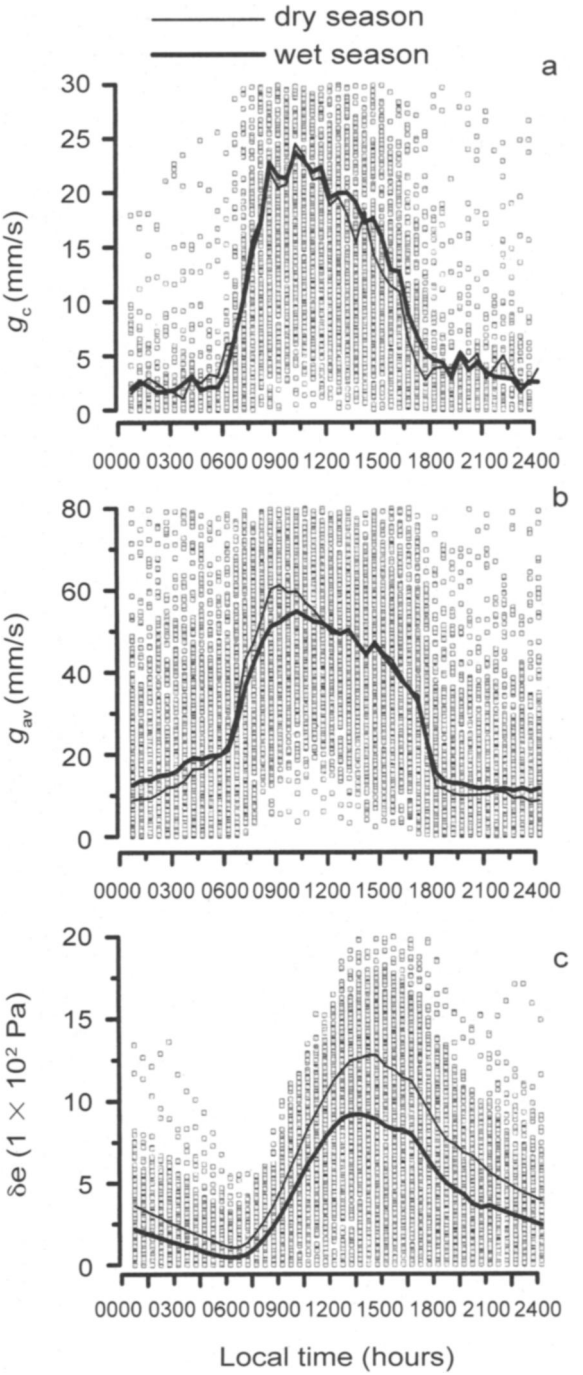

FIG. 11. Diel patterns of (a) surface conductance (g_c), (b) aerodynamic conductance (g_{av}), and (c) water vapor pressure deficit (δe). Note that the scale for δe is in hundreds of pascals. Curves are 30-min means calculated separately for the dry season (thin solid line; 20 July–14 December 2000), and the wet season (thick solid line; 1–13 July 2000 and 15 December 2000–30 June 2001).

ratio, provided that the vapor pressure deficit between the atmosphere and the leaf intercellular spaces remained constant. However, the afternoon decline in Bowen ratio (Fig. 10c) indicates that the afternoon increase in vapor pressure deficit (Fig. 11c) caused by increasing temperature (Fig. 2a) overwhelmed the effect of decreasing in g_c (Fig. 11a).

Conclusion

One of the most striking features of the data set is the lack of evidence for moisture stress during the dry season, an observation that contrasts with previous reports from the Manaus region (Malhi et al. 1998, Williams et al. 1998). The lack of stress is supported by the seasonal patterns of both energy (Figs. 7–11) and CO_2 (Goulden et al. 2004) exchange. Moreover the lack of drought stress is consistent with the observation that ample water remains year round in the soil at depth (Figs. 1e and 3). The lack of stress during the dry season is likely a consequence of deep rooting (Fig. 3), an issue discussed by Nepstad et al. (1994). Additionally, the nocturnal redistribution of water during the dry season may allow the trees to more effectively use the soil water and avoid moisture stress (Figs. 3 and 4). While the forest did not experience appreciable drought stress in 2000–2001, it cannot be concluded that the forest does not become stressed in some years. Annual rainfall exceeded annual evaporation by only 40% (Figs. 1a and 7b). In years with substantially reduced rainfall, as may occur during El Niño periods, increased drought stress is more likely.

Acknowledgments

This work was supported by the U.S. National Aeronautics and Space Administration (Goddard NCC5–280). We thank Marcy Litvak and Antonio Oviedo for help installing equipment; Fernando Leão and Roberto Cardoso for data collection; Cleilim Albert Sousa for field studies; Dan Hodkinson, Bethany Reed, and Lisa Zweede for logistical support; IBAMA, NASA, and INPE for agency support; and many others who provided invaluable advice and support.

Literature Cited

Alvala, R. C. S., R. Gielow, I. R. Wright, and M. G. Hodnett. 1996. Thermal diffusivity of amazonian soils. Pages 139–150 *in* J. H. Gash, C. A. Nobre, J. M. Roberts, and R. L. Victoria, editors. Amazonian deforestation and climate. John Wiley and Sons, Chichester, UK.

Caldwell, M. M., T. E. Dawson, and J. H. Richards. 1998. Hydraulic lift: consequences of water efflux from the roots of plants. Oecologia **113**:151–161.

Culf, A. D., J. L. Esteves, A. O. Marques Filho, and H. R. da Rocha. 1996. Radiation, temperature and humidity over forest and pasture in Amazonia. Pages 175–192 *in* J. H. Gash, C. A. Nobre, J. M. Roberts, and R. L. Victoria, editors. Amazonian deforestation and climate. John Wiley and Sons, Chichester, UK.

da Rocha, H. R., C. A. Nobre, J. P. Bonatti, I. R. Wright, and P. J. Sellers. 1996*a*. A vegetation–atmosphere interaction study for Amazonian deforestation using field data and a single column model. Quarterly Journal of the Royal Meteorological Society **122**:567–598.

da Rocha, H. R., P. J. Sellers, G. J. Collatz, I. R. Wright, and J. Grace. 1996*b*. Calibration and use of the SiB2 model to estimate water vapor and carbon exchange at the ABRACOS forest sites. Pages 459–472 *in* J. H. Gash, C. A. Nobre, J. M. Roberts, and R. L. Victoria, editors. Amazonian deforestation and climate. John Wiley and Sons, Chichester, UK.

Fan, S.-M., S. C. Wofsy, P. S. Bakwin, D. J. Jacob, and D. R. Fitzjarrald. 1990. Atmosphere–biosphere exchange of CO_2 and O_3 in the central-Amazon forest. Journal of Geophysical Research-Atmosphere **95**:16851–16864.

Fitzjarrald, D. R., B. L. Stormwind, G. Fisch, and O. M. R. Cabral. 1988. Turbulent transport observed above the Amazon forest. Journal of Geophysical Research **93**(D2): 1551–1563.

Garratt, J. R. 1992. The atmospheric boundary layer. Cambridge University Press, Cambridge, UK.

Gash, J. C. H., C. A. Nobre, J. M. Roberts, and R. Victória. 1996. Amazonian deforestation and climate. John Wiley and Sons, Chichester, UK.

Goulden, M. L., S. D. Miller, M. C. Menton, H. R. da Rocha, and H. C. de Freitas. 2004. Diel and seasonal patterns of tropical forest CO_2 exchange. Ecological Applications **14**: S42–S54.

Grace, J., J. Lloyd, J. McIntyre, A. Miranda, P. Meir, H. Miranda, J. Moncrieff, J. Massheder, I. Wright, and J. Gash. 1995. Carbon dioxide uptake by an undisturbed tropical rain forest in south-west Amazonia, 1992–1993. Science **270**:778–780.

Hernandez Filho, P., Y. E. Shimabukuro, and D. C. L. Lee. 1993. Final report on the forest inventory project at the Tapajós National Forest. Instituto Nacional de Pesquisas Espaciais, São José dos Campos, SP, Brasil.

Lopes, J. L. M. 2001. Observacoes de umidade do solo em areas de pastagem e floresta em Rondônia utilizando refletometros no dominio da frequencia. Dissertacao de mestrado. Universidade de São Paulo, São Paulo, Brasil.

Malhi, Y., A. D. Nobre, J. Grace, B. Kruijt, M. G. P. Pereira, A. Culf, and S. Scott. 1998. Carbon dioxide transfer over a Central Amazonian rain forest. Journal of Geophysical Research-Atmospheres **103**:31 593–31 612.

McMillen, R. T. 1988. An eddy correlation technique with extended applicability to non-simple terrain. Boundary-Layer Meteorology **43**:231–245.

Miller, S. D., M. L. Goulden, M. C. Menton, H. R. da Rocha, H. C. de Freitas, A. M. e Silva Figueira, and C. A. Dias de Sousa. 2004. Biometric and micrometerological measurements of tropical forest carbon balance. Ecological Applications **14**:S114–S126.

Moore, C. J., and G. F. Fisch. 1996. Estimating heat storage in Amazonian tropical forest. Agricultural Forest Meteorology **38**:147–169.

Nepstad, D. C., C. R. de Carvalho, E. A. Davidson, P. Jipp, P. Lefebvre, G. H. Negreiros, E. D. da Silva, T. Stone, S. Trumbore, and S. Vieira. 1994. The role of deep roots in the hydrological and carbon cycles of Amazonian forests and pastures. Nature **372**:666–669.

Nobre, C. A., P. J. Sellers, and J. Shukla. 1991. Amazonian deforestation and regional climate change. Journal of Climate **4**:957–987.

Peixoto, J. P., and A. Oort. 1994. Physics of climate. American Institute of Physics, New York, New York, USA.

Roberts, J. M., O. M. R. Cabral, G. Fisch, L. C. B. Molion, C. J. Moore, and W. J. Shuttleworth. 1990. Transpiration from an amazonian rainforest calculated from stomatal conductance measurements. Agricultural and Forest Meteorology **65**:175–196.

Sellers, P. J., D. A. Randall, C. J. Collatz, J. A. Berry, C. B. Field, D. A. Dazlich, C. Zhang, and G. D. Collelo. 1996. A revised land surface parameterization (SiB2) for atmospheric GCMs. Part I: model formulation. Journal of Climate **9**:676–705.

Shuttleworth, W. J. 1988. Evaporation from amazonian rain forest. Proceedings of the Royal Society of London Series B **233**:321–346.

Shuttleworth, W. J., et al. 1984. Eddy correlation measurements of energy partition for Amazonian forest. Quarterly Journal of the Royal Meteorological Society **110**:1143–1162.

Stull, R. B. 1993. An introduction to boundary layer meteorology. Kluwer Academic Publishers, Dordrecht, The Netherlands.

Verma, S. B. 1989. Aerodynamic resistances to transfers of heat, mass and momentum in estimation of areal evaporation. Pages 13–20 *in* T. A. Black, D. L. Spittlehouse, M. D. Novak, and D. T. Price, editors. IAHS Publication 177. IAHS Press, Wallingford, UK.

Walter, H. 1984. Vegetation und Klimazonen—Grundriss der globalen Okologie. Eugen Ulmer GmbH, Stuttgart, Germany.

Williams, M., Y. Malhi, A. D. Nobre, E. B. Rastetter, J. Grace, and M. G. P. Pereira. 1998. Seasonal variation in net carbon exchange and evapotranspiration in a Brazilian rain forest: a modeling analysis. Plant Cell and Environment **21**:953–968.

Wofsy, S. C., M. L. Goulden, J. W. Munger, S.-M. Fan, P. S. Bakwin, B. C. Daube, S. L. Bassow, and F. A. Bazzaz. 1993. Net exchange of CO_2 in a mid-latitude forest. Science **260**:1314–1317.